Cell Reports

Report

Preferred inhibition of pro-apoptotic Bak by BclxL via a two-step mechanism

Graphical abstract

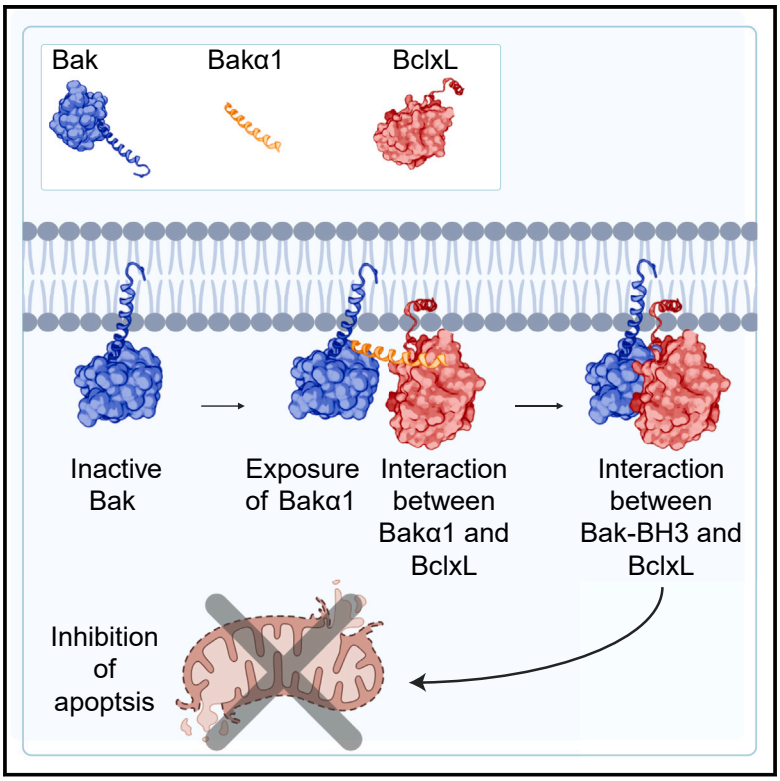

Highlights

- Bakα1 binds to the BH3 binding groove of BclxL with micromolar affinity
- Bakα1 forms an encounter complex with BclxL in the early stages of Bak activation
- The interplay of Bakα1 and BH3 increases the efficiency of inhibition by BclxL

Authors

Kira D. Leitl, Laura E. Sperl, Franz Hagn

Correspondence

franz.hagn@tum.de

In brief

Leitl et al. report on mechanistic details of the inhibition of the pro-apoptotic effector Bcl2 protein Bak by BclxL. Through structural and biophysical investigations, they uncover a second binding site for BclxL on Bak, suggesting a two-step binding model that ensures efficient inhibition of Bak to prevent unwanted pore formation.

Leitl et al., 2024, Cell Reports *43*, 114526
August 27, 2024
https://doi.org/10.1016/j.celrep.2024.114526

CellPress

Cell Reports

CellPress
OPEN ACCESS

Report

Preferred inhibition of pro-apoptotic Bak by BclxL via a two-step mechanism

Kira D. Leitl,[1,2,3] Laura E. Sperl,[1,3] and Franz Hagn[1,2,4,*]
[1]Bavarian NMR Center (BNMRZ), Department of Bioscience, School of Natural Sciences, Technical University of Munich, 85747 Garching, Germany
[2]Molecular Targets and Therapeutics Center (MTTC), Institute of Structural Biology, Helmholtz Munich, 85764 Neuherberg, Germany
[3]These authors contributed equally
[4]Lead contact
*Correspondence: franz.hagn@tum.de
https://doi.org/10.1016/j.celrep.2024.114526

SUMMARY

Bak is a pore-forming Bcl2 protein that induces apoptosis at the outer mitochondrial membrane, which can either proceed via Bak oligomerization or be inhibited by anti-apoptotic Bcl2 proteins, such as BclxL. BclxL is very efficient in inhibiting Bak pore formation, but the mechanistic basis of this preferred interaction has remained enigmatic. Here, we identify Bakα1 as a second binding site for BclxL and show that it specifically interacts with the Bcl2-homology (BH)3 binding groove of BclxL. The affinity between BclxL and Bakα1 is weaker than with Bak-BH3, suggesting that Bakα1, being exposed early in the pore-forming trajectory, transiently captures BclxL, which subsequently transitions to the proximal BH3 site. Bak variants where the initial transient interaction with BclxL is modulated show a markedly altered response to BclxL inhibition. This work contributes to a better mechanistic understanding of the fine-tuned interactions between different players of the Bcl2 protein family.

INTRODUCTION

The induction of apoptosis at the outer mitochondrial membrane (OMM) is regulated by the Bcl2 protein family, which controls OMM permeability via a fine-tuned protein interaction network.[1–5] Effectors, such as Bak, Bax, and Bok, form large pores in the OMM to allow for the exit of apoptotic signaling proteins, such as cytochrome *c*.[6] Bak is largely inactive in healthy cells but under cellular stress can become readily activated by transient interaction with activators (e.g., cBid)[7–11] at the Bak hydrophobic binding groove at the lipid membrane surface.[12–14] Furthermore, it has been recently shown that at higher concentrations, Bak can become auto-active to induce pore formation without stimulation by an activator.[15–17] The pore formation process is nucleated by Bak homo-oligomerization, leading to membrane permeabilization and, ultimately, apoptosis.[18–20] Specifically, the Bak core (α2-5) and latch (α6-8) domains separate upon activation, exposing the so-called Bcl2-homology (BH)3 and BH4 domains.[21,22] Bak then self-assembles into a dimer via the pairwise interaction between the BH3 domains and the hydrophobic groove of two Bak molecules,[23,24] followed by the formation of an oligomeric pore in the membrane consisting of multiple dimer units.[25–27] However, in the absence of cellular stress, the Bak-BH3 domain is readily engaged by anti-apoptotic Bcl2 proteins such as BclxL via its hydrophobic BH3 binding groove that is oriented toward the membrane surface,[28] leading to an inhibition of Bak dimerization and, consequently, pore formation[2,3,5,29] (Figure 1A). It has been well established that to undergo activation, Bak residues 1–66 (spanning α1 and the loop region to α2) within the BH4 domain adopt a flexible random coil structure[17,29,30] and become solvent exposed.[13,17,31–33] From this point, the BH3-mediated homo-dimerization and subsequent pore formation of Bak is in a direct competition with its inhibition by anti-apoptotic Bcl2 proteins, such as BclxL, that bind to the Bak-BH3 domain with high affinity.[34] Previous studies have postulated an interaction between BclxL and the N-terminal region of the effector Bcl2 protein Bax,[35,36] although the interaction surface and the mechanistic implications remained controversial. Furthermore, it has been suggested that the efficient inhibition of Bak by BclxL might be caused by the availability of a second binding site.[29] Despite these initial insights, our understanding of the structural and mechanistic basis of this preferred interaction remains sparse.

Here, we used nuclear magnetic resonance (NMR) spectroscopy, hydrogen-deuterium exchange mass spectrometry (HDX-MS), and other biophysical methods to identify Bakα1 as a second binding site for BclxL. As probed by NMR chemical shift perturbation (CSP) experiments, Bakα1 interacts with the canonical BH3 binding groove in BclxL. Pore-forming assays in liposomes showed that Bakα1 was able to inhibit complex formation between Bak and BclxL, suggesting a competitive binding scenario. However, in contrast to Bak-BH3, Bakα1 was unable to directly activate Bak pore formation in liposomes. The binding affinity between BclxL and Bakα1 is markedly weaker than that of the Bak-BH3 domain, suggesting that the transient Bakα1-BclxL interaction is readily dissociated once the BH3 site becomes exposed. This idea is corroborated with pore-forming assay data using Bak variants where α1 is either removed or fused with an additional high-affinity BH3 site, leading to a reduction of the inhibition

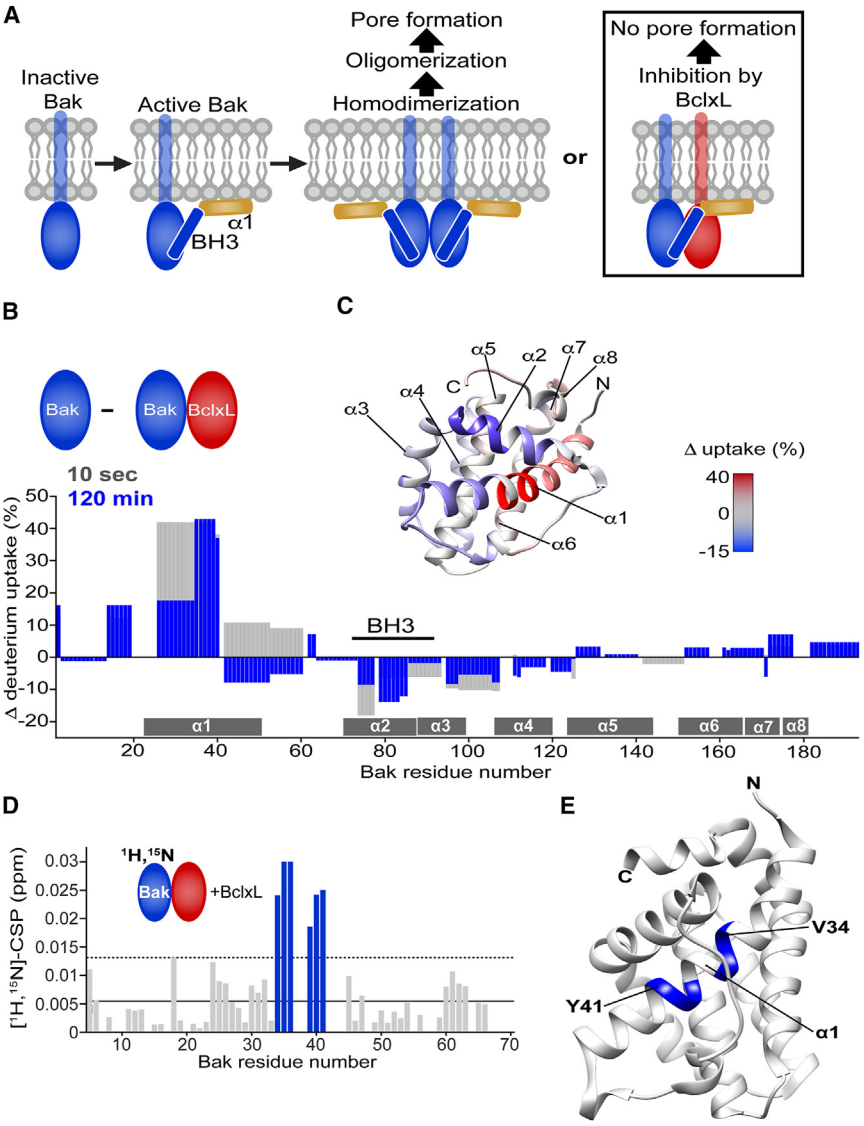

Figure 1. Interaction of Bak and BclxL at the membrane surface probed by HDX-MS and NMR

(A) Model of Bak conformational changes enabling pore formation and inhibition by BclxL. Upon activation of Bak (blue), Bakα1 (orange) detaches, unfolds, and binds to the membrane surface to stabilize the active Bak intermediate, followed by homo-dimerization and pore formation. Inhibition of Bak by BclxL (red) is finally achieved by binding to the Bak-BH3 domain.

(B) HDX-MS-detected differences in hydrogen exchange of BakΔTM versus BakΔTM in the presence of excess BclxLΔTM in liposomes in technical triplicates. The data are plotted against the sequence of BakΔTM at time points of 10 s (gray) and 120 min (blue).

(C) Data from (B) color coded onto the structure of BakΔTM for the final time point of 120 min. Residues in Bakα1 show strongly reduced exchange in the complex with BclxL, implying an interaction site. The parts of BakΔTM that putatively form a membrane pore are more protected from the solvent without BclxLΔTM.

(D) Chemical shift perturbation (CSP) plot extracted from 2D-[^{15}N, ^{1}H]-TROSY spectra of BakΔTM bound to nanodiscs with or without BclxLΔTMΔHis$_6$ after heat-induced activation. The most significant CSPs (mean value, solid line; mean value plus standard deviation, broken line) as well as residues that disappeared upon the addition of BclxLΔTM (CSP set to 0.03 ppm) are shown in dark blue.

(E) Data from (D) mapped onto the structure of BakΔTM. The affected residues (V34-Y41) align well with the interaction pattern obtained by HDX-MS (B and C).

See also Figures S1 and S2.

by BclxL at equimolar concentrations. This set of data suggests a sequential binding mechanism where the solvent-accessible α1 of activated Bak engages in an encounter complex with BclxL, followed by a transition to the exposed high-affinity Bak-BH3 site. This study provides structural evidence for the preferred interaction between Bak and BclxL and explains why, even in the presence of excess high-affinity BH3-only proteins, BclxL is still able to partially inhibit Bak.

RESULTS

BclxL interacts with an early Bak activation intermediate

To probe the interaction between Bak and BclxL at the lipid bilayer membrane surface, we first used HDX-MS. In these experiments, we attached C-terminally His-tagged soluble domains of Bak and BclxL (BakΔTM and BclxLΔTM, respectively) to liposomes assembled with an *E. coli* polar lipid blend doped with 5% Ni-NTA lipids to ensure a stable attachment of both proteins to the membrane surface in a native-like correct orientation. Since a high concentration of BakΔTM (>500 nM) was used as well as a negatively charged lipid blend that enhances pore-forming activity,[17] its activation did not require the addition of an activator BH3-only protein.[17,37] HDX experiments have been previously used to detect the unfolding of the Bak N-terminal region upon activation.[17,30] Using this setup, the difference in the degree of deuterium uptake of BakΔTM in the free versus BclxLΔTM-bound form were analyzed at different time points, ranging from 10 s to 120 min (Figure 1B; Figure S1). At the 10 s exchange time, it can be readily seen that the relative degree of hydrogen exchange of residues 26–40 in Bakα1 is reduced by around 40% in the presence of BclxLΔTM, indicating a protection of the exchangeable protons caused by the interaction with BclxLΔTM. The degree of protection by BclxLΔTM stays very similar even after 2 h (blue bars in Figure 1B), with more selective protection at the C-terminal half (aa 35–40) of Bakα1. The difference in deuterium

uptake at the 2 h time point is color coded on the folded BakΔTM structure in Figure 1C. The very C-terminal end of α1 (aa 40–47) as well as the short α-helical regions between α1 and the BH3 region (aa 48–60) are initially more protected in the complex with BclxLΔTM but show higher protection without BclxLΔTM after 120 min, presumably due to the involvement of these regions in the oligomeric and membrane-embedded BakΔTM pore structure. Even though a recent structure of the BakΔTM core homo-dimer (aa 67–147) does not contain this region,[23] protection by membrane proximity of this peptide stretch right next to the putative pore structure seems very likely. Furthermore, large parts of BakΔTM (including the BH3 domain, aa 74–88, and the rest of the core dimer up to ~aa 140) show a higher protection without BclxLΔTM, which most likely represents the difference in membrane location where a BakΔTM pore is less exposed than a partly folded BakΔTM in complex with BclxLΔTM on the membrane surface. In these experiments, we do not see additional protection of the BH3 domain by BclxLΔTM, which is the canonical high-affinity binding site, but rather higher protection without BclxL. A likely explanation for this is the formation of a Bak homo-dimer where the BH3 domain is an integral part of the dimerization interface, leading to strong protection. In order to validate these results at higher resolution, we used NMR with *U*-[^{2}H,^{15}N]-labeled BakΔTM attached to lipid nanodiscs via Ni-NTA lipids[38,39] alone or in the presence of a 10-fold molar excess of BclxLΔTM without the C-terminal His tag. This setup was necessary to prevent competition of Bak and BclxL for the Ni-NTA-binding sites of the nanodisc. Due to the smaller size and stronger confinement of nanodiscs compared to liposomes, auto-activation of BakΔTM at higher protein concentrations does not occur but requires the addition of BH3-only activators such as cBid.[17] However, since the presence of excess BH3-only proteins would also lead to BclxL inhibition,[40,41] we instead used heat (40°C for 30 min) to activate BakΔTM.[42] Subsequently, 2D-[^{15}N, ^{1}H]-TROSY spectra were recorded for both samples. NMR chemical shift information for the visible N-terminal region (aa 1–66) of activated BakΔTM was reported previously[17] (BMRB: 50942). In these experiments, we could detect selective CSPs in Bakα1 induced by the presence of BclxLΔTM (Figures 1D and 1E; Figure S2). In addition, residues F35 and R36 were broadened beyond detection, which was considered a strong binding effect (maximum bar heights in Figure 1D). Regions showing CSPs and line broadening are in a peptide stretch between V34 and Y41 (Figures 1D and 1E), which aligns very well with the interaction pattern obtained by HDX-MS (Figures 1B and 1C).

Bakα1 specifically binds to the canonical binding site of BclxL

Next, we validated the interaction between Bak and BclxL in a simplified setup using Bakα1 instead of the entire soluble domain. For recombinant production of Bakα1, we used a fusion protein of Bakα1 (E24-E48) and the protein G B1 domain (GB1). To obtain interaction information at a per-residue resolution, we used our previously obtained NMR chemical shift assignments of activated BakΔTM at the membrane surface[17] and additionally performed a set of 3D triple-resonance experiments (HNCO, HN(CA)CO, HNCA, and HNCACB) to transfer the published assignments to the GB1-Bakα1 construct used here. The quality of the 3D NMR spectra was sufficient to assign 84% of the backbone amide resonances of the peptide, with only two missing residues at each of the N- and C-terminal ends. We then monitored binding between the ^{15}N-labeled GB1-Bakα1 and BclxLΔTM by recording 2D-[^{15}N, ^{1}H]-HSQC NMR spectra of 110 μM GB1-Bakα1 alone or after the addition of a 6-fold molar excess of unlabeled BclxLΔTM (Figure 2A; Figure S3). The interaction with BclxLΔTM caused severe line broadening in the HSQC spectrum of Bakα1 in a continuous peptide stretch between residues V34 and H43, as indicated in the sequence (Figure 2A) and structure (Figure 2B) of Bakα1. This interaction site is in good agreement with the NMR and HDX-MS data of the entire Bak soluble domain (Figure 1). No pronounced spectral perturbations were seen in any resonances originating from GB1, highlighting the specificity of the interaction. After the successful confirmation of the binding site at Bakα1, we next performed NMR experiments to probe the binding site for Bakα1 on BclxLΔTM. For this, we recorded 2D-[^{15}N, ^{1}H]-HSQC spectra with 250 μM *U*-[^{2}H,^{15}N]-labeled BclxLΔTM in the presence or absence of a 10-fold molar excess of GB1-Bakα1 (Figure 2C; Figure S4). Using the previously published NMR backbone resonance chemical shift information for BclxLΔTM[43] (BMRB: 25466), we could assign strong CSPs within BclxLΔTM for residues in the region spanning α2-5 and α8, which cover the BH1, BH2, and BH3 domains (Figures 2C and 2D) that form the canonical binding site for BH3 peptides.[5,28,29,34]

Next, we aimed at constructing a structural model of the BclxL-Bakα1 complex based on the CSP data obtained by NMR and molecular dynamics (MD) simulations (Figure 3A). After extracting the structure of Bakα1 (residues 24–48) from the published Bak crystal structure (PDB: 2IMS[44]), we first performed a structural alignment of regions in Bakα1 that showed CSPs with the structure of BclxL bound to Bak-BH3 (PDB: 1BXL[34]). This procedure resulted in a reasonable binding pose that is consistent with the NMR data. To further equilibrate that structural model, we performed an extended 3 μs MD simulation, which resulted in a stable structural state (stable root-mean-square deviation [RMSD] relative to the starting structure) after approximately 2 μs simulation time (Figure 3B, left) and led to the unfolding of terminal parts of Bakα1 that are not in contact with BclxL, as indicated by a large root-mean-square fluctuation (RMSF) value. The residues in Bakα1 that interact with BclxL (E32-Q44) remained α-helical in the MD simulation (low RMSF values), giving rise to an amphipathic α-helix, as also seen in the BclxL-Bak-BH3 complex[34] (Figure 3B, right). As expected from the NMR data, the docking model shows that Bakα1 interacts with the hydrophobic BH3 binding groove of BclxLΔTM (Figure 3C). However, the orientation of the peptide relative to BclxL could not be defined by these NMR data. To experimentally validate the head-to-head orientation in our docking model, we next conducted paramagnetic relaxation enhancement (PRE) NMR experiments, where the spatial proximity of a spin label in Bakα1 in the complex will lead to NMR signal attenuation of the ^{1}H,^{15}N resonances in BclxL. We designed two individual Bakα1 peptides containing single cysteines at positions 27 or 47 (V27C, Q47C) and attached a PROXYL spin label to each peptide. These two positions are adjacent to, but not within, the

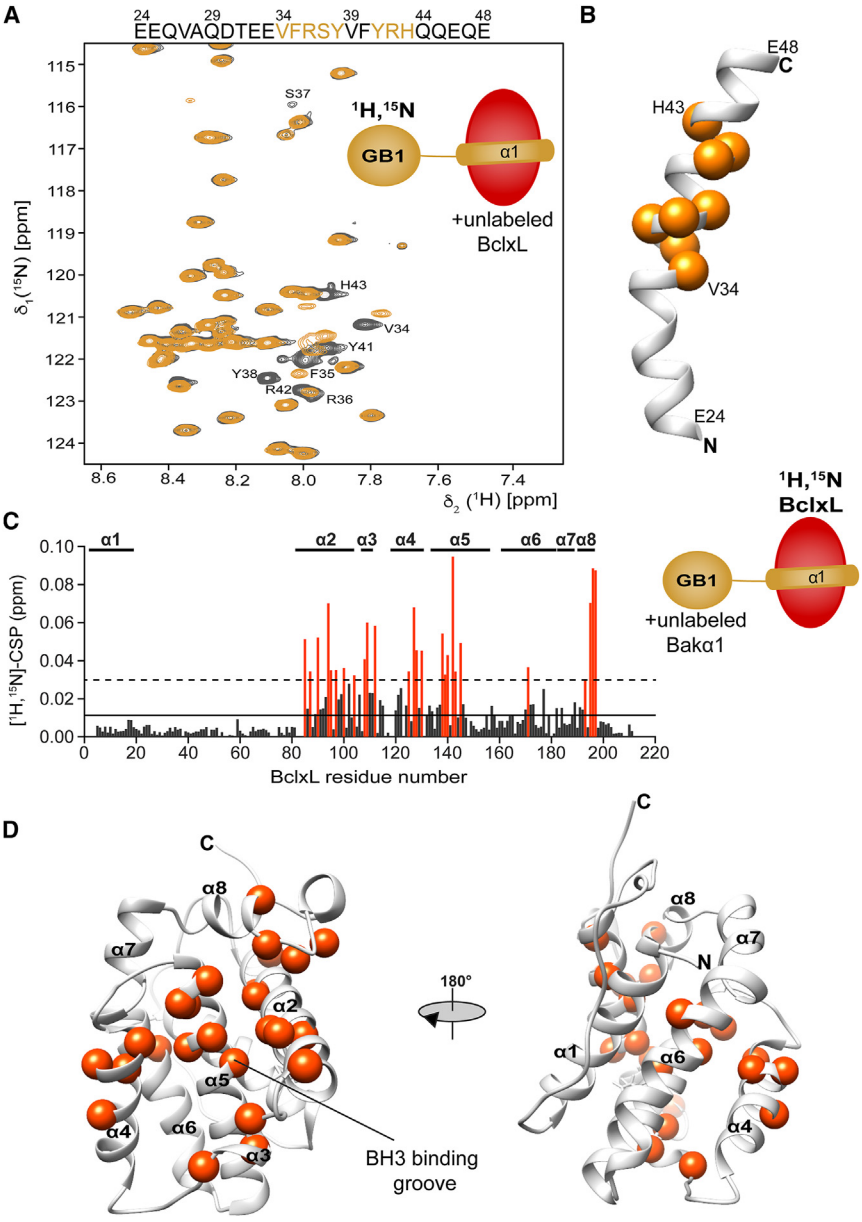

Figure 2. Bakα1 binds to the hydrophobic binding groove of BclxL

(A) NMR spectral overlay of Bakα1 (gray) and Bakα1 + BclxLΔTM (orange) in 2D-[^{15}N, ^{1}H]-HSQC spectra. NMR backbone resonance assignments are indicated on the spectral overlay for the most significant CSPs that are marked in orange in the primary sequence.

(B) Data from (A) mapped onto the structure of Bakα1. The most significant CSPs are shown as orange spheres.

(C) CSP plot from 2D-[^{15}N, ^{1}H]-HSQC spectra of BclxLΔTM ± Bakα1. The most significant CSPs (mean value, solid line; plus standard deviation, broken line) are indicated in red.

(D) Data from (C) mapped onto the structure of BclxLΔTM. The most significant CSPs are shown as red spheres.

See also Figures S3 and S4A.

determined binding site (V34-H43) in Bakα1, ensuring that the spin label does not interfere with the interaction. 2D-[^{15}N, ^{1}H]-HSQC spectra of *U*-[^{2}H,^{15}N]-BclxLΔTM in complex with spin-labeled Bakα1-V27C or Bakα1-Q47C were recorded before and after the addition of an excess of ascorbic acid to quench the unpaired electron of the spin label. The PRE effect was visualized by the obtained intensity ratio (± ascorbic acid) for each amino acid in BclxLΔTM (Figure S5A). Since position 47 in Bakα1 is closer to the proposed binding site, we could observe a more pronounced PRE effect on the NMR signals of residues in BclxL located at the canonical hydrophobic BH3 binding groove. In addition, PRE effects with Bakα1-Q47C also appeared in α8 at the C terminus of BclxLΔTM, indicating that the spin label in Bakα1 is near this region. These data suggest that the C terminus of Bakα1 is oriented toward the C terminus of BclxLΔTM, which is in line with the canonical binding mode of BH3 peptides to BclxL.[34] Our complex structural model shows binding of the amphipathic Bakα1 peptide to the hydrophobic BH3 binding groove of BclxL, with charged or polar residues pointing toward the solvent (Figure 3D, left).

To validate our binding model further, we mutated Bakα1 at residue F35 (F35A), which is oriented toward the hydrophobic binding pocket of BclxL and broadened beyond detection in our NMR titration experiments. In addition, F35 engages in an anion-π interaction with E129 of BclxL (Figure 3D, right). Glu-Phe anion-π interactions are reported to be highly abundant in proteins.[45] We determined the binding affinity of wild-type (Bakα1-wt) or Bakα1-F35A for BclxLΔTM using a series of 2D-[^{15}N, ^{1}H]-HSQC NMR experiments with 350 μM *U*-[^{15}N]-BclxLΔTM in the presence of increasing concentrations of either GB1-Bakα1 peptide (150–2,000 μM; Figure 3E, left). The CSP values of selected resonances in the BH3 binding groove of BclxLΔTM (A89, L94, F150) were plotted against the concentration of Bakα1 to obtain a binding isotherm (Figure 3E, right; Figure S5B), yielding a dissociation constant (K_D) of 450 μM for Bakα1-wt and 1.3 mM for Bakα1-F35A (Figure 3F), indicating an almost 3-fold decrease in affinity caused by this single point mutation.

Bakα1 inhibits the anti-pore-forming activity of BclxL in a lipid environment

To elucidate the interaction of Bakα1 and BclxL in a functional context, we conducted an established liposome permeabilization assay.[46,47] In these experiments, we monitored the pore-forming

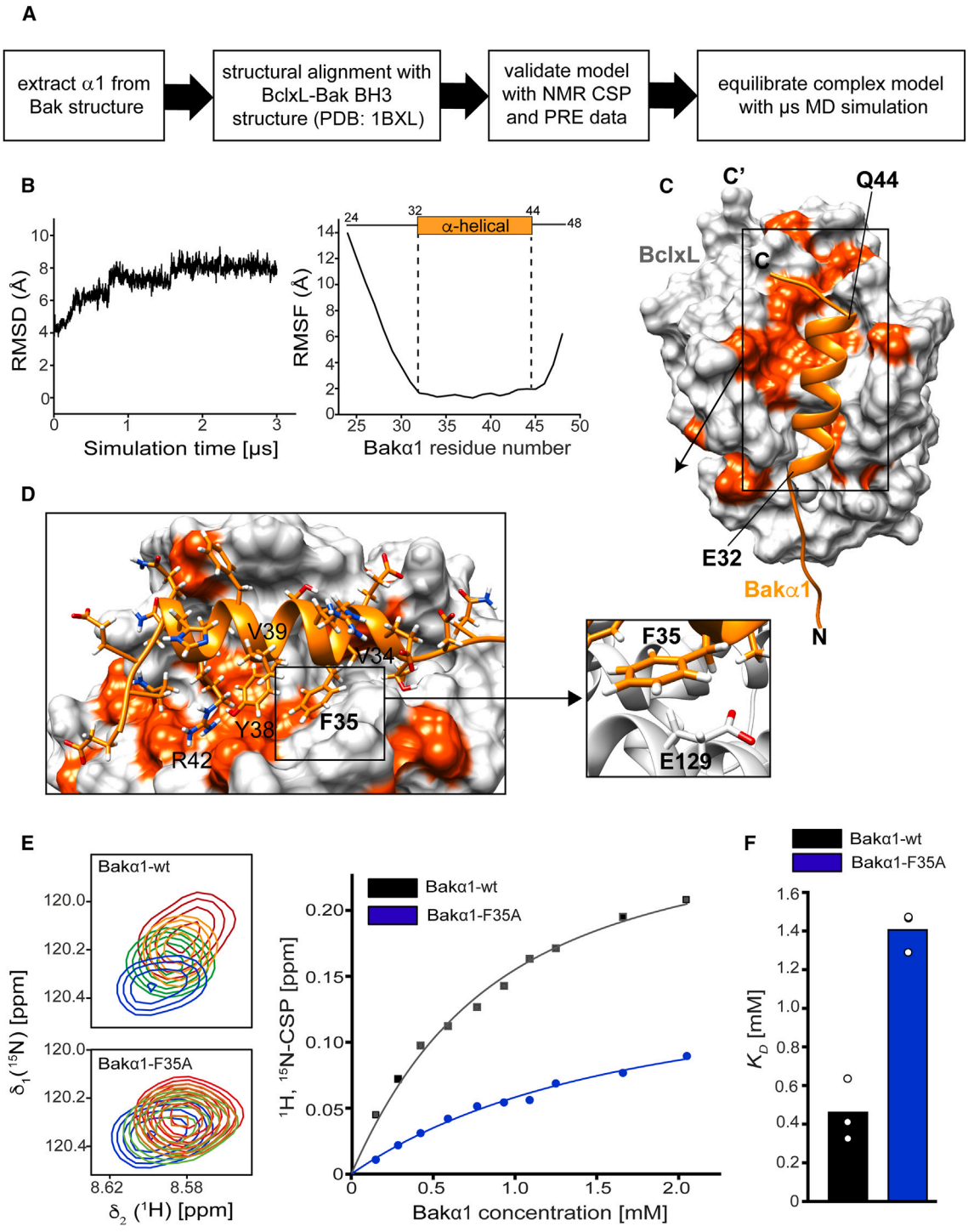

Figure 3. Complex structural model of BclxL bound to Bakα1

(A) Workflow for the generation of a complex structural model of Bakα1 and BclxLΔTM using NMR data and computational tools.

(B) Left: root-mean-square deviation (RMSD) of the BclxL-Bakα1 complex during the 3 μs MD simulation. After 2 μs, a stable conformation was populated. Right: root-mean-square fluctuation (RMSF) of Bakα1 in the docking model during the 3 μs MD simulation indicating that the binding residues 32–44 remain rigid in the complex.

(C) Complex structural model of BclxLΔTM and Bakα1 obtained by the outlined protocol (A). NMR CSPs are indicated by red color on the surface representation of BclxL.

(legend continued on next page)

activity of BakΔTM under auto-activation conditions (high Bak concentration of 1 μM) where no activator BH3-only protein was necessary[17,37] (Figure 4A). As expected, BclxLΔTM can inhibit the pore-forming activity of BakΔTM even at a sub-stoichiometric ratio (1 μM BakΔTM:500 nM BclxLΔTM, Figure 4A). We used this assay setup to quantify the binding of Bakα1 to BclxLΔTM, which would lead to a concentration-dependent restoration of Bak pore formation due to the dissociation of the Bak-BclxL complex by competitive binding of Bakα1 to the BclxL BH3 site (Figure 4A). A titration series with up to 100 μM Bakα1 yielded an increase in Bak-mediated pore formation in a concentration-dependent manner (Figure 4B), characterized by an inhibitory concentration (IC_{50}) of ~67 μM (inset in Figure 4B).

Next, we wondered whether Bakα1 might also act as a direct activator for Bak, such as Bak BH3[16] or the BH3-only protein cBid. To investigate this question, we employed a pore-forming liposome assay at a lower BakΔTM concentration (200 nM) where an activator protein is needed to stimulate pore formation. As expected, 50 nM of cBid was sufficient to activate BakΔTM and induce pore formation (Figure 4C). In contrast, the addition of Bakα1 (10–200 μM) was not able to stimulate pore formation (Figure 4C; Figure S6), indicating that Bakα1 does not function as an activator of Bak but rather serves as an interaction site for anti-apoptotic BclxL.

A sequential binding model explains the preferred interaction between Bak and BclxL

After having identified and validated a second binding site in Bak for BclxL, we next wondered how this finding can be rationalized in a mechanistic manner. To address this question, we determined the binding affinity of Bakα1 for BclxLΔTM using a series of 2D-[^{15}N, ^{1}H]-HSQC NMR experiments with 120 μM *U*-[^{15}N]-GB1-Bakα1 in the presence of increasing concentrations of BclxLΔTM (60–1,100 μM). The CSPs of resonances in Bakα1, which are in the central binding motif in our complex structural model were plotted against the concentration of BclxLΔTM to obtain a binding isotherm (Figure 5A), yielding a K_D of 114 μM. This affinity is approximately two times weaker than that determined in the liposome pore-forming assay (Figures 4A and 4B), which can be rationalized by the use of membrane-attached proteins in the assay that lead to a high local concentration of the protein components, which was absent in the NMR titration experiments. The high-affinity residues in Bakα1 (F35, Y38) located at the same side of the α-helix (Figure 3D) are flanked by low-affinity (~1 mM) residues (Figure S7), suggesting that these residues form the core interaction motif in Bakα1. To compare the affinity obtained by NMR for Bakα1 with Bak-BH3, we performed a similar NMR titration series with *U*-[^{15}N]-GB1-Bakα1-BH3. The resulting concentration-dependent CSP values of select resonances within Bak-BH3 plotted against the BclxLΔTM concentration indicated strong binding (Figure 5B) with an extracted K_D value of ~2 μM, which is close to value reported in the literature.[34] In addition, isothermal titration calorimetry (ITC) experiments were conducted with GB1-Bakα1-BH3 or GB1-Bak-BH3 and BclxLΔTM. The binding isotherms obtained with both Bak constructs were nearly identical (K_D = ~30 nM), suggesting that the high-affinity BH3 domain dominates the binding process (Figure S8A). In addition to the ITC experiments, we used ^{15}N-labeled GB1-Bak constructs (GB1-Bakα1 and GB1-Bakα1-BH3) and performed NMR-detected titration experiments with unlabeled BclxLΔTM (Figure S8B). Looking at residues in α1 (V34, Y41, R42), we could see that CSPs were observed with Bakα1 readily upon the addition of BclxL, consistent with a specific interaction. However, in the Bakα1-BH3 construct, marked CSPs could only be detected for these residues in α1 once the high-affinity BH3 binding site was saturated by BclxL at the equivalence point of 350 μM, indicating that BclxL will bind to Bak-BH3 once it becomes exposed during activation.

To explore the impact of Bakα1 on the potency of Bak inhibition by BclxL in a pore-forming liposome assay, we designed a construct (BakΔTMΔα1) where Bakα1 could be cleaved off via an engineered thrombin site in the loop between α1 and α2. This strategy ensures that BakΔTMΔα1 can be produced as a folded protein and readily digested before the assay. Inhibition of BakΔTM (1 μM) by BclxLΔTM (125–500 nM) was highly efficient even at 8-fold lower concentrations of BclxLΔTM than BakΔTM (125 nM versus 1 μM; Figures 5C and 5E, gray). In contrast, when α1 was removed from BakΔTM by pre-treatment with thrombin, the sensitivity to inhibition by BclxLΔTM was greatly reduced, with more than 4 times higher BclxLΔTM concentrations (>500 nM) required for full inhibition than for BakΔTM-WT (Figures 5C and 5E, blue). These results align very well with our findings that two binding sites on Bak contribute to the interaction with BclxL. To further rationalize the notion that high- and low-affinity binding sites in Bak are indeed necessary for productive inhibition by BclxL, we designed a construct (BakΔTM-Bad-BH3) where we added a high-affinity binding site for BclxL to the N terminus of Bak. Specifically, the BH3 domain of the BH3-only protein Bad (aa 140–165) that binds to BclxL with a K_D value of ~6 nM[48] was added. In this extended BakΔTM construct, the Bad BH3 domain is exposed and accessible for binding to BclxL even without Bak activation. All Bak variants used for the described pore-forming assays were properly folded as indicated by circular dichroism (CD) spectroscopy and size-exclusion chromatography (Figure S9). In our pore-forming assay, we found that Bak inhibition by BclxLΔTM occurred only partially up to a 1:1 stoichiometry (Figures 5D–5F, blue). An excess concentration of BclxL

(D) Enlarged interaction site between BclxL and Bakα1 showing that Baka1 forms an amphipathic helix and engages in hydrophobic interactions with BclxL. F35 in Bakα1 forms an anion-π interaction with E129 in BclxL.
(E) Left: NMR spectral overlays from NMR titration experiments of BclxLΔTM (blue; residue L94) and BclxLΔTM + Bakα1 (green to red) in 2D-[^{15}N, ^{1}H]-HSQC spectra using Bakα1-wt (top) and Bakα1-F35A (bottom). Right: CSPs for BclxLΔTM residue L94 were plotted at increasing Bakα1 concentrations and used for curve fitting and the extraction of a K_D value.
(F) Comparison of K_D values for Bakα1-wt (black) and Bakα1-F35A (blue) upon binding to BclxLΔTM. Three BclxLΔTM residues (A89, L94, F150) were used for error analysis as technical replicates. Individual data points for each residue are shown as black circles.
See also Figures S4B, S5B, and S7.

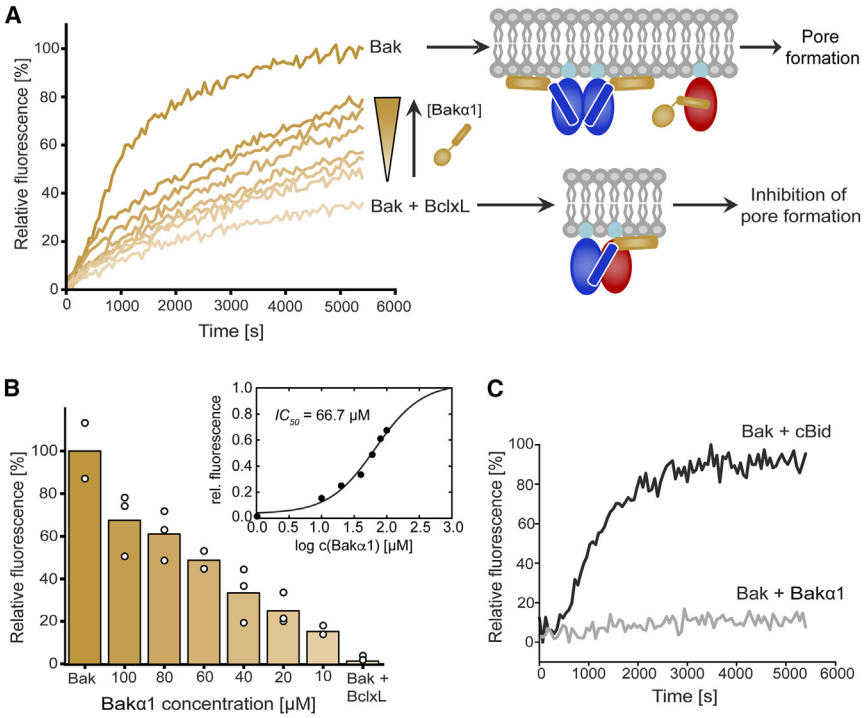

Figure 4. Bakα1 can dissociate the BclxL-Bak complex as probed by pore formation assays

(A) Pore formation in liposomes mediated by BakΔTM auto-activation at 1 μM concentration (orange) or after the addition of BclxLΔTM at inhibiting concentrations (500 nM, light beige). Titration of Bakα1 (up to 100 μM, light beige to orange) to the Bak-BclxL complex re-establishes pore formation in a concentration-dependent manner. A cartoon model of the mode of action of the role of Bakα1 in the initial activation steps of Bak is depicted on the right.

(B) Normalized fluorescence intensities of the data shown in (A) at 5,500 s. Individual data points are shown as black circles. Data analysis was conducted on three technical replicates unless clear outliers were removed. These data provided an IC_{50} value of ~67 μM (inset).

(C) BakΔTM pore formation at a concentration of 200 nM requires activation, as seen for the BH3-only protein cBid (50 nM, black). In contrast, even 200 μM of Bakα1 was unable to activate BakΔTM (gray).

See also Figure S6.

(>1 μM) was required for full inhibition, with maximal inhibition visible at ~1.5 μM for BakΔTM-Bad-BH3 versus 0.5 μM for BakΔTM-wt (Figures 5D–5F). This finding clearly shows that the presence of a second readily accessible high-affinity binding site in Bak prevents BclxL from interacting with the Bak-BH3 domain that is only exposed upon Bak activation. Thus, the lower affinity of Bakα1 is essential to (1) enhance the affinity between Bak and BclxL and (2) enable the transition of BclxL to the final BH3 site to inhibit its oligomerization and, ultimately, pore formation.

DISCUSSION

It is well established that BH3-only proteins act on effectors such as Bak in a "hit-and-run" mechanism of activation.[7–11] In addition, Bak activation can be induced by higher Bak concentrations on the membrane surface by auto-activation, as seen in our liposome permeabilization assay data (Figures 4A, 5C, and 5D; Figure S6) and in previous studies.[15–17] Anti-apoptotic proteins are proposed to inhibit apoptosis by way of two mechanisms[29,48,49]: (1) binding to BH3-only proteins and/or (2) binding to pro-apoptotic effectors after they are activated. It seems plausible that the latter mechanism is more efficient since the effector Bcl2 proteins are captured directly. Thus, it has been suggested that effector Bcl2 proteins (Bak, Bax) can engage in a preferred interaction with the anti-apoptotic members, such as BclxL.[29] Until now, it has been speculated that the interaction between the anti-apoptotic proteins and effector proteins extends outside of the canonical BH3 domain,[35,36] potentially explaining the increased efficiency of direct inhibition.[29] Our study now provides clear structural and functional evidence of a binding site for BclxL at Bakα1 via residues V34-H43 that interact with low affinity with the canonical hydrophobic binding groove of BclxL. These findings are consistent with *in vivo* data on the other Bcl2 effector protein Bax, where an antibody recognizing the N terminus of active Bax was not able to bind in the presence of BclxL.[36] The primary sequence conservation between Bax and Bak in α1 is not very high, yet is more pronounced than between Bak and the BH3-activator protein Bid. Our experimental data also agree with a recent computational study where Baxα1 was shown to interact with BclxL.[35] However, in contrast to this computation study, our experimental data clearly show that the canonical BH3 binding groove, not the first α-helix of BclxL, mediates the interaction. Our set of structural and functional data suggests a model (Figure 5G) where the initially exposed α1 of activated Bak rapidly engages in a dynamic encounter complex with BclxL. Once captured, BclxL can transition from the exposed low-affinity Bakα1 to the more buried high-affinity Bak-BH3 site to prevent Bak homo-dimerization and oligomeric pore formation. By this mechanism, binding of BclxL to the sterically more shielded BH3 binding site becomes kinetically favored. These data provide evidence for why, even in the presence of high-affinity BH3-only proteins,[10,50] BclxL is still able to inhibit Bak. In line with this model, our liposome permeabilization data on a Bak construct lacking α1 show a decrease in BclxL inhibition efficiency (Figures 5C–5E). However, the encounter complex with α1 apparently needs to be transient and weak to allow for the transition of BclxL to the final high-affinity BH3 site. Our assay results with Bak containing an N-terminally exposed high-affinity Bad-BH3 domain clearly show that the inhibition of pore formation by BclxL is drastically reduced if the initial interaction is equally strong (Figures 5D–5F).

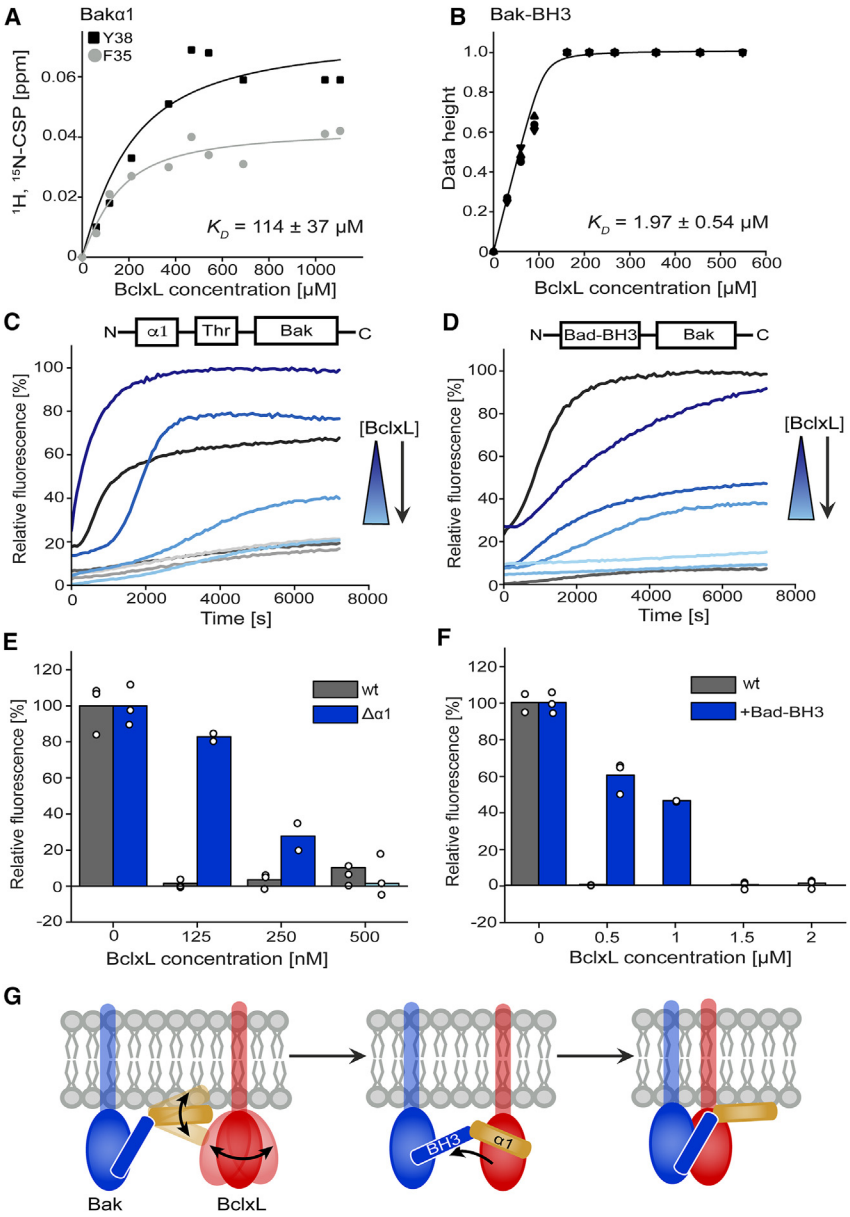

Figure 5. Sequential binding of Bak by BclxL

(A and B) NMR titration analysis to assess binding of Bakα1 and Bakα1-BH3 to BclxLΔTM. CSPs for select residues in (A) Bakα1 (Y38, black; F35, gray) and (B) Bak-BH3 (4 individual residues in BH3 domain as technical replicates) were plotted at increasing BclxLΔTM concentrations and used for data fitting and the extraction of a K_D value. The data for Bak-BH3 residues are represented as the normalized data height due to severe line broadening in the presence of BclxLΔTM.

(C) Pore formation in liposomes mediated by Bak auto-activation at 1 μM concentration with either BakΔTM (black) or BakΔTMΔα1 (dark blue). Titration of BclxLΔTM (black to light gray) at inhibiting concentrations (up to 500 nM) readily led to inhibition of BakΔTM, whereas inhibition of BakΔTMΔα1 (dark to light blue) required a more than 4-fold higher BclxLΔTM concentration. Data analysis was conducted on three technical replicates unless clear outliers due to experimental artifacts were removed.

(D) Pore formation in liposomes mediated by Bak auto-activation at 1 μM concentration with either BakΔTM (black) or BakΔTM fused with an N-terminal Bad-BH3 domain (BakΔTM-Bad-BH3; dark blue). The addition of BclxLΔTM (gray) at inhibiting concentrations (0.5 μM) readily led to abolished pore formation of BakΔTM, whereas the onset of inhibition of BakΔTM-Bad-BH3 (dark to light blue) only started at excess concentrations of BclxLΔTM. Data analysis was conducted on three technical replicates unless clear outliers due to experimental artifacts were removed.

(E) Normalized fluorescence intensities of the data shown in (C) at 5,500 s. Individual data points are shown as black circles.

(F) Normalized fluorescence intensities of the data shown in (D) at 5,500 s. Individual data points are shown as black circles.

(G) Sequential binding model of Bak inhibition. Bak (blue) activation begins with Bakα1 (orange) unfolding and attaching to the membrane surface. The dynamic Bakα1 signals Bak activation and sequesters BclxL (red). The C-terminal half of Bakα1 (V34-Q44) transiently captures BclxL at the membrane surface, where BclxL then transitions to the high-affinity Bak-BH3 domain to efficiently inhibit Bak.

See also Figures S8 and S9.

Transient protein-protein interactions are important for many aspects of cellular function, although their characterization remains challenging, especially for *in vitro* analysis.[51] Furthermore, unfolded regions are especially important in facilitating transient protein-protein interactions.[52] In contrast to its interaction with BclxL, Bakα1 does not activate Bak, which is consistent with an *in vivo* proteolytic study showing that Bakα1 is not necessary for inducing pore formation.[30] Thus, it can be postulated that Bakα1, once exposed, exclusively facilitates the interaction with anti-apoptotic Bcl2 proteins to favor the inhibition of pore formation. This study provides important insights into the preferred interaction between effector Bcl2 proteins and anti-apoptotic members. Our findings can inform therapeutic approaches aimed at selective activation of apoptosis by specifically targeting Bakα1. One approach could be the use of the monoclonal antibody 6A7, which has an epitope at the N terminus of the effector Bax.[36] In line with our assay data and existing *in vivo* data, treatment with this antibody could block the initial binding of BclxL to the activated effector protein and encourage apoptosis.[36]

Limitations of the study

In this study, we did not work with the full-length constructs of both BclxL and Bak due to challenges in working with proteins containing transmembrane helices (TMHs), as well as uncontrolled membrane insertion of Bak during the longer sample preparation procedures of the full-length protein by, e.g., SortaseA ligation.[28] Therefore, the impact of the TMHs of both BclxL

and Bak on the interaction described here remain to be investigated. However, it seems unlikely that the TMHs interact, given that their amino acid sequences are almost identical and oligomerization has not been observed for BclxL-TMH.[53] Furthermore, a more thorough mutagenesis study with Bak to abolish the interaction with BclxL is limited because mutations in, e.g., Bakα1 and BH3 will strongly alter its stability, folding state, and pore-forming activity *in vitro* and *in vivo*.

STAR★METHODS

Detailed methods are provided in the online version of this paper and include the following:

- KEY RESOURCES TABLE
- RESOURCE AVAILABILITY
  - Lead contact
  - Materials availability
  - Data and code availability
- METHOD DETAILS
  - Protein expression and purification
  - Preparation of liposomes
  - Preparation of phospholipid nanodiscs
  - Liposome permeabilization assay
  - Hydrogen deuterium exchange mass spectrometry (HDX-MS)
  - Isothermal titration calorimetry (ITC)
  - Circular dichroism (CD) spectroscopy
  - NMR spectroscopy
  - Molecular docking
- QUANTIFICATION AND STATISTICAL ANALYSIS
  - Liposome permeabilization assay data analysis
  - ITC data analysis
  - NMR spectroscopy data analysis

SUPPLEMENTAL INFORMATION

Supplemental information can be found online at https://doi.org/10.1016/j.celrep.2024.114526.

ACKNOWLEDGMENTS

HDX-MS experiments were performed by Florian Rührnößl at the Center for Functional Protein Assemblies at the Technical University of Munich supported by the DFG (CRC1035, project Z1, project number 201302640). All NMR experiments were conducted at the Bavarian NMR Center (BNMRZ) supported by the Technical University of Munich and Helmholtz Munich. Drs. Gerd Gemmecker and Sam Asami are gratefully acknowledged for general NMR support.

AUTHOR CONTRIBUTIONS

K.D.L. conducted liposome permeabilization assay experiments, ITC measurements, Bakα1 backbone resonance assignment experiments, and NMR titrations with Bakα1 mutants, analyzed data, and wrote the manuscript. L.E.S. conducted NMR titration experiments, HDX-MS, and NMR-PRE experiments and analyzed data. F.H. acquired funding, designed research, analyzed data, and wrote the manuscript. All authors commented on and approved the manuscript.

DECLARATION OF INTERESTS

The authors declare no competing interests.

Received: February 27, 2024
Revised: June 14, 2024
Accepted: July 8, 2024

REFERENCES

1. Bock, F.J., and Tait, S.W.G. (2020). Mitochondria as multifaceted regulators of cell death. Nat. Rev. Mol. Cell Biol. *21*, 85–100. https://doi.org/10.1038/s41580-019-0173-8.
2. Chipuk, J.E., Moldoveanu, T., Llambi, F., Parsons, M.J., and Green, D.R. (2010). The BCL-2 family reunion. Mol. Cell *37*, 299–310. https://doi.org/10.1016/j.molcel.2010.01.025.
3. Czabotar, P.E., Lessene, G., Strasser, A., and Adams, J.M. (2014). Control of apoptosis by the BCL-2 protein family: implications for physiology and therapy. Nat. Rev. Mol. Cell Biol. *15*, 49–63. https://doi.org/10.1038/nrm3722.
4. Green, D.R. (2005). Apoptotic pathways: ten minutes to dead. Cell *121*, 671–674. https://doi.org/10.1016/j.cell.2005.05.019.
5. Moldoveanu, T., Follis, A.V., Kriwacki, R.W., and Green, D.R. (2014). Many players in BCL-2 family affairs. Trends Biochem. Sci. *39*, 101–111. https://doi.org/10.1016/j.tibs.2013.12.006.
6. Garrido, C., Galluzzi, L., Brunet, M., Puig, P.E., Didelot, C., and Kroemer, G. (2006). Mechanisms of cytochrome c release from mitochondria. Cell Death Differ. *13*, 1423–1433. https://doi.org/10.1038/sj.cdd.4401950.
7. Brouwer, J.M., Lan, P., Cowan, A.D., Bernardini, J.P., Birkinshaw, R.W., van Delft, M.F., Sleebs, B.E., Robin, A.Y., Wardak, A., Tan, I.K., et al. (2017). Conversion of Bim-BH3 from Activator to Inhibitor of Bak through Structure-Based Design. Mol. Cell *68*, 659–672.e9. https://doi.org/10.1016/j.molcel.2017.11.001.
8. Hockings, C., Anwari, K., Ninnis, R.L., Brouwer, J., O'Hely, M., Evangelista, M., Hinds, M.G., Czabotar, P.E., Lee, E.F., Fairlie, W.D., et al. (2015). Bid chimeras indicate that most BH3-only proteins can directly activate Bak and Bax, and show no preference for Bak versus Bax. Cell Death Dis. *6*, e1735. https://doi.org/10.1038/cddis.2015.105.
9. Leshchiner, E.S., Braun, C.R., Bird, G.H., and Walensky, L.D. (2013). Direct activation of full-length proapoptotic BAK. Proc. Natl. Acad. Sci. USA *110*, E986–E995. https://doi.org/10.1073/pnas.1214313110.
10. Letai, A., Bassik, M.C., Walensky, L.D., Sorcinelli, M.D., Weiler, S., and Korsmeyer, S.J. (2002). Distinct BH3 domains either sensitize or activate mitochondrial apoptosis, serving as prototype cancer therapeutics. Cancer Cell *2*, 183–192. https://doi.org/10.1016/s1535-6108(02)00127-7.
11. Wei, M.C., Lindsten, T., Mootha, V.K., Weiler, S., Gross, A., Ashiya, M., Thompson, C.B., and Korsmeyer, S.J. (2000). tBID, a membrane-targeted death ligand, oligomerizes BAK to release cytochrome c. Genes Dev. *14*, 2060–2071.
12. Bleicken, S., Hantusch, A., Das, K.K., Frickey, T., and Garcia-Saez, A.J. (2017). Quantitative interactome of a membrane Bcl-2 network identifies a hierarchy of complexes for apoptosis regulation. Nat. Commun. *8*, 73. https://doi.org/10.1038/s41467-017-00086-6.
13. Moldoveanu, T., Grace, C.R., Llambi, F., Nourse, A., Fitzgerald, P., Gehring, K., Kriwacki, R.W., and Green, D.R. (2013). BID-induced structural changes in BAK promote apoptosis. Nat. Struct. Mol. Biol. *20*, 589–597. https://doi.org/10.1038/nsmb.2563.
14. O'Neill, K.L., Huang, K., Zhang, J., Chen, Y., and Luo, X. (2016). Inactivation of prosurvival Bcl-2 proteins activates Bax/Bak through the outer mitochondrial membrane. Genes Dev. *30*, 973–988. https://doi.org/10.1101/gad.276725.115.
15. Iyer, S., Uren, R.T., Dengler, M.A., Shi, M.X., Uno, E., Adams, J.M., Dewson, G., and Kluck, R.M. (2020). Robust autoactivation for apoptosis by BAK but not BAX highlights BAK as an important therapeutic target. Cell Death Dis. *11*, 268. https://doi.org/10.1038/s41419-020-2463-7.
16. Singh, G., Guibao, C.D., Seetharaman, J., Aggarwal, A., Grace, C.R., McNamara, D.E., Vaithiyalingam, S., Waddell, M.B., and Moldoveanu, T. (2022). Structural basis of BAK activation in mitochondrial apoptosis initiation. Nat. Commun. *13*, 250. https://doi.org/10.1038/s41467-021-27851-y.
17. Sperl, L.E., Ruhrnossl, F., Schiller, A., Haslbeck, M., and Hagn, F. (2021). High-resolution analysis of the conformational transition of pro-apoptotic

Bak at the lipid membrane. EMBO J. *40*, e107159. https://doi.org/10.15252/embj.2020107159.

18. Chipuk, J.E., and Green, D.R. (2008). How do BCL-2 proteins induce mitochondrial outer membrane permeabilization? Trends Cell Biol. *18*, 157–164. https://doi.org/10.1016/j.tcb.2008.01.007.
19. Uren, R.T., Iyer, S., and Kluck, R.M. (2017). Pore formation by dimeric Bak and Bax: an unusual pore? Philos. Trans. R. Soc. Lond. B Biol. Sci. *372*, 20160218. https://doi.org/10.1098/rstb.2016.0218.
20. Uren, R.T., O'Hely, M., Iyer, S., Bartolo, R., Shi, M.X., Brouwer, J.M., Alsop, A.E., Dewson, G., and Kluck, R.M. (2017). Disordered clusters of Bak dimers rupture mitochondria during apoptosis. Elife *6*, e19944. https://doi.org/10.7554/eLife.19944.
21. Brouwer, J.M., Westphal, D., Dewson, G., Robin, A.Y., Uren, R.T., Bartolo, R., Thompson, G.V., Colman, P.M., Kluck, R.M., and Czabotar, P.E. (2014). Bak core and latch domains separate during activation, and freed core domains form symmetric homodimers. Mol. Cell *55*, 938–946. https://doi.org/10.1016/j.molcel.2014.07.016.
22. Czabotar, P.E., Westphal, D., Dewson, G., Ma, S., Hockings, C., Fairlie, W.D., Lee, E.F., Yao, S., Robin, A.Y., Smith, B.J., et al. (2013). Bax crystal structures reveal how BH3 domains activate Bax and nucleate its oligomerization to induce apoptosis. Cell *152*, 519–531. https://doi.org/10.1016/j.cell.2012.12.031.
23. Birkinshaw, R.W., Iyer, S., Lio, D., Luo, C.S., Brouwer, J.M., Miller, M.S., Robin, A.Y., Uren, R.T., Dewson, G., Kluck, R.M., et al. (2021). Structure of detergent-activated BAK dimers derived from the inert monomer. Mol. Cell *81*, 2123–2134.e5. https://doi.org/10.1016/j.molcel.2021.03.014.
24. Dewson, G., Kratina, T., Sim, H.W., Puthalakath, H., Adams, J.M., Colman, P.M., and Kluck, R.M. (2008). To trigger apoptosis, Bak exposes its BH3 domain and homodimerizes via BH3:groove interactions. Mol. Cell *30*, 369–380. https://doi.org/10.1016/j.molcel.2008.04.005.
25. Dewson, G., Kratina, T., Czabotar, P., Day, C.L., Adams, J.M., and Kluck, R.M. (2009). Bak activation for apoptosis involves oligomerization of dimers via their alpha6 helices. Mol. Cell *36*, 696–703. https://doi.org/10.1016/j.molcel.2009.11.008.
26. Westphal, D., Dewson, G., Czabotar, P.E., and Kluck, R.M. (2011). Molecular biology of Bax and Bak activation and action. Biochim. Biophys. Acta *1813*, 521–531. https://doi.org/10.1016/j.bbamcr.2010.12.019.
27. Westphal, D., Kluck, R.M., and Dewson, G. (2014). Building blocks of the apoptotic pore: how Bax and Bak are activated and oligomerize during apoptosis. Cell Death Differ. *21*, 196–205. https://doi.org/10.1038/cdd.2013.139.
28. Raltchev, K., Pipercevic, J., and Hagn, F. (2018). Production and Structural Analysis of Membrane-Anchored Proteins in Phospholipid Nanodiscs. Chemistry *24*, 5493–5499. https://doi.org/10.1002/chem.201800812.
29. Llambi, F., Moldoveanu, T., Tait, S.W., Bouchier-Hayes, L., Temirov, J., McCormick, L.L., Dillon, C.P., and Green, D.R. (2011). A unified model of mammalian BCL-2 protein family interactions at the mitochondria. Mol. Cell *44*, 517–531. https://doi.org/10.1016/j.molcel.2011.10.001.
30. Sandow, J.J., Tan, I.K., Huang, A.S., Masaldan, S., Bernardini, J.P., Wardak, A.Z., Birkinshaw, R.W., Ninnis, R.L., Liu, Z., Dalseno, D., et al. (2021). Dynamic reconfiguration of pro-apoptotic BAK on membranes. EMBO J. *40*, e107237. https://doi.org/10.15252/embj.2020107237.
31. Alsop, A.E., Fennell, S.C., Bartolo, R.C., Tan, I.K., Dewson, G., and Kluck, R.M. (2015). Dissociation of Bak α1 helix from the core and latch domains is required for apoptosis. Nat. Commun. *6*, 6841. https://doi.org/10.1038/ncomms7841.
32. Griffiths, G.J., Dubrez, L., Morgan, C.P., Jones, N.A., Whitehouse, J., Corfe, B.M., Dive, C., and Hickman, J.A. (1999). Cell damage-induced conformational changes of the pro-apoptotic protein Bak in vivo precede the onset of apoptosis. J. Cell Biol. *144*, 903–914. https://doi.org/10.1083/jcb.144.5.903.
33. Iyer, S., Anwari, K., Alsop, A.E., Yuen, W.S., Huang, D.C., Carroll, J., Smith, N.A., Smith, B.J., Dewson, G., and Kluck, R.M. (2016). Identification of an activation site in Bak and mitochondrial Bax triggered by antibodies. Nat. Commun. *7*, 11734. https://doi.org/10.1038/ncomms11734.
34. Sattler, M., Liang, H., Nettesheim, D., Meadows, R.P., Harlan, J.E., Eberstadt, M., Yoon, H.S., Shuker, S.B., Chang, B.S., Minn, A.J., et al. (1997). Structure of Bcl-xL-Bak peptide complex: recognition between regulators of apoptosis. Science *275*, 983–986. https://doi.org/10.1126/science.275.5302.983.
35. Ding, J., Mooers, B.H.M., Zhang, Z., Kale, J., Falcone, D., McNichol, J., Huang, B., Zhang, X.C., Xing, C., Andrews, D.W., and Lin, J. (2014). After embedding in membranes antiapoptotic Bcl-XL protein binds both Bcl-2 homology region 3 and helix 1 of proapoptotic Bax protein to inhibit apoptotic mitochondrial permeabilization. J. Biol. Chem. *289*, 11873–11896. https://doi.org/10.1074/jbc.M114.552562.
36. Hsu, Y.T., and Youle, R.J. (1997). Nonionic detergents induce dimerization among members of the Bcl-2 family. J. Biol. Chem. *272*, 13829–13834. https://doi.org/10.1074/jbc.272.21.13829.
37. Oh, K.J., Singh, P., Lee, K., Foss, K., Lee, S., Park, M., Lee, S., Aluvila, S., Park, M., Singh, P., et al. (2010). Conformational changes in BAK, a pore-forming proapoptotic Bcl-2 family member, upon membrane insertion and direct evidence for the existence of BH3-BH3 contact interface in BAK homo-oligomers. J. Biol. Chem. *285*, 28924–28937. https://doi.org/10.1074/jbc.M110.135293.
38. Hagn, F., Nasr, M.L., and Wagner, G. (2018). Assembly of phospholipid nanodiscs of controlled size for structural studies of membrane proteins by NMR. Nat. Protoc. *13*, 79–98. https://doi.org/10.1038/nprot.2017.094.
39. Günsel, U., and Hagn, F. (2022). Lipid Nanodiscs for High-Resolution NMR Studies of Membrane Proteins. Chem. Rev. *122*, 9395–9421. https://doi.org/10.1021/acs.chemrev.1c00702.
40. Pogmore, J.P., Pemberton, J.M., Chi, X., and Andrews, D.W. (2016). Using Förster-Resonance Energy Transfer to Measure Protein Interactions Between Bcl-2 Family Proteins on Mitochondrial Membranes. Methods Mol. Biol. *1419*, 197–212. https://doi.org/10.1007/978-1-4939-3581-9_15.
41. Yao, Y., Bobkov, A.A., Plesniak, L.A., and Marassi, F.M. (2009). Mapping the interaction of pro-apoptotic tBID with pro-survival BCL-XL. Biochemistry *48*, 8704–8711. https://doi.org/10.1021/bi901171n.
42. Pagliari, L.J., Kuwana, T., Bonzon, C., Newmeyer, D.D., Tu, S., Beere, H.M., and Green, D.R. (2005). The multidomain proapoptotic molecules Bax and Bak are directly activated by heat. Proc. Natl. Acad. Sci. USA *102*, 17975–17980. https://doi.org/10.1073/pnas.0506712102.
43. Yao, Y., Fujimoto, L.M., Hirshman, N., Bobkov, A.A., Antignani, A., Youle, R.J., and Marassi, F.M. (2015). Conformation of BCL-XL upon Membrane Integration. J. Mol. Biol. *427*, 2262–2270. https://doi.org/10.1016/j.jmb.2015.02.019.
44. Moldoveanu, T., Liu, Q., Tocilj, A., Watson, M., Shore, G., and Gehring, K. (2006). The X-ray structure of a BAK homodimer reveals an inhibitory zinc binding site. Mol. Cell *24*, 677–688. https://doi.org/10.1016/j.molcel.2006.10.014.
45. Lucas, X., Bauza, A., Frontera, A., and Quinonero, D. (2016). A thorough anion-pi interaction study in biomolecules: on the importance of cooperativity effects. Chem. Sci. *7*, 1038–1050. https://doi.org/10.1039/c5sc01386k.
46. Kale, J., Chi, X., Leber, B., and Andrews, D. (2014). Examining the molecular mechanism of bcl-2 family proteins at membranes by fluorescence spectroscopy. Methods Enzymol. *544*, 1–23. https://doi.org/10.1016/B978-0-12-417158-9.00001-7.
47. Yethon, J.A., Epand, R.F., Leber, B., Epand, R.M., and Andrews, D.W. (2003). Interaction with a membrane surface triggers a reversible conformational change in Bax normally associated with induction of apoptosis. J. Biol. Chem. *278*, 48935–48941. https://doi.org/10.1074/jbc.M306289200.
48. Kelekar, A., Chang, B.S., Harlan, J.E., Fesik, S.W., and Thompson, C.B. (1997). Bad is a BH3 domain-containing protein that forms an inactivating

dimer with Bcl-XL. Mol. Cell Biol. *17*, 7040–7046. https://doi.org/10.1128/MCB.17.12.7040.

49. Leber, B., Lin, J., and Andrews, D.W. (2010). Still embedded together binding to membranes regulates Bcl-2 protein interactions. Oncogene *29*, 5221–5230. https://doi.org/10.1038/onc.2010.283.
50. Happo, L., Strasser, A., and Cory, S. (2012). BH3-only proteins in apoptosis at a glance. J. Cell Sci. *125*, 1081–1087. https://doi.org/10.1242/jcs.090514.
51. Perkins, J.R., Diboun, I., Dessailly, B.H., Lees, J.G., and Orengo, C. (2010). Transient protein-protein interactions: structural, functional, and network properties. Structure *18*, 1233–1243. https://doi.org/10.1016/j.str.2010.08.007.
52. Uversky, V.N. (2015). Functional roles of transiently and intrinsically disordered regions within proteins. FEBS J. *282*, 1182–1189. https://doi.org/10.1111/febs.13202.
53. Hausler, E., Fredriksson, K., Goba, I., Peters, C., Raltchev, K., Sperl, L., Steiner, A., Weinkauf, S., and Hagn, F. (2020). Quantifying the insertion of membrane proteins into lipid bilayer nanodiscs using a fusion protein strategy. Biochim. Biophys. Acta Biomembr. *1862*, 183190. https://doi.org/10.1016/j.bbamem.2020.183190.
54. Hagn, F., Klein, C., Demmer, O., Marchenko, N., Vaseva, A., Moll, U.M., and Kessler, H. (2010). BclxL changes conformation upon binding to wild-type but not mutant p53 DNA binding domain. J. Biol. Chem. *285*, 3439–3450. https://doi.org/10.1074/jbc.M109.065391.
55. Battiste, J.L., and Wagner, G. (2000). Utilization of site-directed spin labeling and high-resolution heteronuclear nuclear magnetic resonance for global fold determination of large proteins with limited nuclear overhauser effect data. Biochemistry *39*, 5355–5365. https://doi.org/10.1021/bi000060h.
56. Sattler, M., Schleucher, J., and Griesinger, C. (1999). Heteronuclear multidimensional NMR experiments for the structure determination of proteins in solution employing pulsed field gradients. Prog. Nucl. Magn. Reson. Spectrosc. *34*, 93–158. https://doi.org/10.1016/S0079-6565(98)00025-9.
57. Pettersen, E.F., Goddard, T.D., Huang, C.C., Couch, G.S., Greenblatt, D.M., Meng, E.C., and Ferrin, T.E. (2004). UCSF Chimera–a visualization system for exploratory research and analysis. J. Comput. Chem. *25*, 1605–1612. https://doi.org/10.1002/jcc.20084.
58. Jo, S., Kim, T., Iyer, V.G., and Im, W. (2008). CHARMM-GUI: a web-based graphical user interface for CHARMM. J. Comput. Chem. *29*, 1859–1865. https://doi.org/10.1002/jcc.20945.
59. Lee, J., Cheng, X., Swails, J.M., Yeom, M.S., Eastman, P.K., Lemkul, J.A., Wei, S., Buckner, J., Jeong, J.C., Qi, Y., et al. (2016). CHARMM-GUI Input Generator for NAMD, GROMACS, AMBER, OpenMM, and CHARMM/OpenMM Simulations Using the CHARMM36 Additive Force Field. J. Chem. Theor. Comput. *12*, 405–413. https://doi.org/10.1021/acs.jctc.5b00935.
60. Humphrey, W., Dalke, A., and Schulten, K. (1996). VMD: visual molecular dynamics. J. Mol. Graph. *14*, 33–38. https://doi.org/10.1016/0263-7855(96)00018-5.
61. Abraham, M.J., Murtola, T., Schulz, R., Páll, S., Smith, J.C., Hess, B., and Lindahl, E. (2015). GROMACS: High performance molecular simulations through multi-level parallelism from laptops to supercomputers. SoftwareX *1–2*, 19–25. https://doi.org/10.1016/j.softx.2015.06.001.
62. Farmer, B.T., 2nd, Constantine, K.L., Goldfarb, V., Friedrichs, M.S., Wittekind, M., Yanchunas, J., Jr., Robertson, J.G., and Mueller, L. (1996). Localizing the NADP+ binding site on the MurB enzyme by NMR. Nat. Struct. Biol. *3*, 995–997. https://doi.org/10.1038/nsb1296-995.
63. Fielding, L. (2007). NMR methods for the determination of protein-ligand dissociation constants. Prog. Nucl. Magn. Reson. Spectrosc. *51*, 219–242. https://doi.org/10.1016/j.pnmrs.2007.04.001.

STAR★METHODS

KEY RESOURCES TABLE

REAGENT or RESOURCE	SOURCE	IDENTIFIER
Bacterial and virus strains		
Escherichia coli BL21(DE3)	Thermo Fisher	Cat#EC0114
Escherichia coli BL21-XL10	Agilent Technologies	Cat#200315
Chemicals, peptides, and recombinant proteins		
BakΔTM	Sperl et al.[17]	N/A
BclxLΔTM	Hagn et al.[54]	N/A
BakΔTMΔα1	This paper	N/A
BakΔTM-Bad-BH3	This paper	N/A
GB1-Bakα1	This paper	N/A
GB1-Bakα1-BH3	This paper	N/A
cBid	Sperl et al.[17]	N/A
TEV protease	Hagn lab	N/A
Thrombin	Cytiva	Cat#27084601
GB1-Bak-BH3	This paper	NA
Isopropyl β-D-thiogalactosidase (IPTG), powder	Sigma-Aldrich	Cat#I6758
DNase I, Grade II, from bovine pancreas	Sigma-Aldrich	Cat#10104159001
Tris(hydroxymethyl)aminomethane	SERVA	Cat#37190.03
LB (Luria Bretani) broth, Miller (granulated)	VWR	Cat#85856.5000
Liver L-α-phosphatidylinositol (PI)	Avanti Polar Lipids	Cat#840042C
18:1 1,2-dioleyl-*sn*-glycero-3-phospho-L-serine (DOPS)	Avanti Polar Lipids	Cat#840035C
1,1′,2,2′-tetra-(9Z-octadecenoyl)cardiolipin	Avanti Polar Lipids	Cat#710335C
Egg L-α-phosphatidylcholine (PC)	Avanti Polar Lipids	Cat#840051C
18:1 DGS-NTA(Ni)	Avanti Polar Lipids	Cat#790404P
Glycerol	Sigma-Aldrich	Cat#G6279
cOmplete, EDTA-free New Protease Inhibitor Cocktail Tablets provided in glass vials	Sigma-Aldrich	Cat#05056489001
L-L-α-phosphatidylethanolamine (PE)	Avanti Polar Lipids	Cat#840021C
Sodium phosphate dibasic	Sigma-Aldrich	Cat#S3264
β-mercaptoethanol (BME)	AppliChem	Cat#A1108
Dithiothreitol (DTT)	Panreac AppliChem	Cat#A1101
Tris(2-carboxyethyl)phosphine (TCEP)	Sigma-Aldrich	Cat#C4706
2-[4-(2-hydroxyethyl)piperazin-1-yl]ethanesulfonic acid (HEPES)	VWR	Cat#0511
Sodium chloride	VWR	Cat#1064045000
Potassium chloride	Carl Roth	Cat#6781.1
Sodium phosphate monobasic	Sigma-Aldrich	Cat#S8282
Ethylenediaminetetraacetic acid (EDTA)	Panreac AppliChem	Cat#A1103,1000
Imidazole	Panreac AppliChem	Cat#A1073,1000
Ampicillin sodium salt	Carl Roth	Cat#HP62.2
Magnesium chloride	Carl Roth	Cat#KK36.1
Sodium cholate	Thermo Fisher	Cat#A17074-18
Phenylmethansulfonylfluoride (PMSF)	Sigma-Aldrich	Cat#329-98-6
Bio-Beads SM-2	Bio-Rad	Cat#1523920
E. coli extract polar lipids	Avanti Polar Lipids	Cat#100600C
Calcium chloride	Sigma-Aldrich	Cat#C1016

(*Continued on next page*)

Continued

REAGENT or RESOURCE	SOURCE	IDENTIFIER
Potassium phosphate monobasic	Sigma-Aldrich	Cat#795488
Sodium phosphate dibasic	Sigma-Aldrich	Cat#S3264
Ammonium-15N chloride, powder, 98%	Sigma-Aldrich	Cat#299251
(+)-Biotin	Sigma-Aldrich	Cat#B4501
Thiamine hydrochloride	VWR	Cat#28605.180
Magnesium sulfate	Sigma-Aldrich	Cat#M2643
D-(+)-Glucose	Sigma-Aldrich	Cat#G7021
D-Glucose (U-13C6, 99%)	Eurisotope	Cat#CLM-1396
Deuterium oxide, 99.9%	Sigma-Aldrich	Cat#151882
Boric acid	Sigma-Aldrich	Cat#B6768
Zinc chloride	Carl Roth	Cat#3533.1
Iron(II) chloride tetrahydrate	Carl Roth	Cat#1H93.3
Sodium molybdate dihydrate	Carl Roth	Cat#0274.4
Manganese(II) chloride tetrahydrate	Sigma-Aldrich	Cat#221279
Cobalt(II) chloride hexahydrate	Carl Roth	Cat#7095.1
Copper(II) chloride dihydrate	Carl Roth	Cat#CN82.3
GB1-Bakα1-F35A	This paper	N/A
Critical commercial assays		
Pfu DNA polymerase	Promega	Cat#M7741
QuikChange Lightning Site-Directed Mutagenesis Kit	Agilent	Cat#210518
Deposited data		
BclxLΔTM backbone resonance chemical shift assignment	Yao et al.[43]	BMRB accession code 25466
BakΔTM backbone resonance chemical shift assignment	Sperl et al.[17]	BMRB accession code 50942
Oligonucleotides		
Primers for PCR	See Table S1	N/A
Recombinant DNA		
pET21a-BakΔTM-His6	Sperl et al.[17]	N/A
pET21a-BclxLΔTM-His6	Hagn et al.[54]	N/A
pET21a-cBid-His6	Sperl et al.[17]	N/A
pET21a-Bakα1-Thr-BakΔTM-His6	This paper	N/A
pET21a-BadBH3-BakΔTM-His6	This paper	N/A
pET21a-His6-TEV-GB1-Thr-Bakα1	This paper	N/A
pET21a-His6-TEV-GB1-Thr-Bakα1-BakBH3	This paper	N/A
pET21a-His6-TEV-GB1-Thr-BakBH3	This paper	N/A
pET21a-His6-TEV-GB1-Thr-Bakα1(F35A)	This paper	N/A
Software and algorithms		
Topspin 3.5pL6	Bruker	https://www.bruker.com/en/products-and-solutions/mr/nmr-software.html
OriginPro, Version 2021b	OriginLab Corporation	https://www.originlab.com/index.aspx?go=Products/Origin
Adobe Illustrator CS6	Adobe Systems Incorporated	https://www.adobe.com/products/illustrator.html
Jasco Spectra Manager	JASCO	https://jascoinc.com/products/spectroscopy/molecular-spectroscopy-software/
MicroCal PEAQ-ITC software	Malvern Panalytical	https://www.malvernpanalytical.com/en/support/product-support/software/microcal-peaq-itc-analysis-software-v141
NMR-FAM Sparky 1.413	NMRFAM	https://www.cgl.ucsf.edu/home/sparky/

(*Continued on next page*)

Continued

REAGENT or RESOURCE	SOURCE	IDENTIFIER
UCSF Chimera	University of California	https://www.cgl.ucsf.edu/chimera/
Unicorn 7.1	Cytiva	https://www.cytivalifesciences.com/en/us/shop/chromatography/software/unicorn-7-p-05649
BioRender 2024	BioRender	https://www.biorender.com/
CcpNmr Analysis 2.4.2	CCPN	https://ccpn.ac.uk/software/version-2/
GROMACS Version 2023.3	GROMACS	https://manual.gromacs.org/2023.3/index.html
CHARMM-GUI server	Lehigh University	https://www.charmm-gui.org/?doc=about
VMD	University of Illinois	https://www.ks.uiuc.edu/Research/vmd/
PLGS 3.0.3	Waters	https://www.waters.com/waters/library.htm?cid=511436&lid=134899946&lcid=134899945
DynamX 3.0	Waters	https://www.waters.com/waters/library.htm?locale=en_US&lid=134832928
Other		
HiLoad 16/600 Superdex 75 pg preparative size exclusion chromatography column	Cytiva	Cat#28989334
HiLoad 16/600 Superdex 200 pg preparative size exclusion chromatography column	Cytiva	Cat#28989335
NAP-5 purification columns	Cytiva	Cat#17085302
Ni Sepharose excel purification resin	Cytiva	Cat#17371202
ACQUITY UPLC BEH C18 column, 1.7 μm, 2.1 mm × 100 mm	Waters	SKU#176000864
ACQUITY Premier CSH C18 column with Vanguard FIT, 1.7 μm, 2.1 mm × 100 mm	Waters	SKU#186009464
Enzymate protein pepsin column, 5 μm, 2.1 mm × 30 mm	Waters	SKU#186007233

RESOURCE AVAILABILITY

Lead contact

Further information and requests for resources should be directed to the lead contact, Dr. Franz Hagn (franz.hagn@tum.de).

Materials availability

Plasmids used from this study will be available by request with some restrictions (MTA completion).

Data and code availability

- This study did not generate any deposited data.
- This paper does not report original code.
- Any additional information required to reanalyze the data reported in this paper is available from the lead contact (Dr. Franz Hagn, franz.hagn@tum.de) upon request.

METHOD DETAILS

Protein expression and purification

Plasmid constructs encoding for the soluble domains of Bak (BakΔTM) and BclxL (BclxLΔTM) were cloned and expressed in *E. coli* as previously described.[17,28,44,54] A cBid construct was cloned and expressed in *E. coli* as previously described. In the resulting cBid protein, a thrombin cleavage site is replacing the original caspase-8 site.[17] Purification of BakΔTM, BclxLΔTM and cBid was done as described previously.[17] A construct where Bakα1 can be removed proteolytically (BakΔTMΔα1) was designed by inserting a thrombin cleavage site and adjacent linker residues (amino acid residues: EGYDELVPRGSRSSHSRLG) after BakΔTM Leu65 and removing Gln66. Purification of BakΔTMΔα1 was identical to the procedure for BakΔTM. Following size exclusion chromatography (SEC), thrombin was added (1:40 M ratio) to selected fractions and incubated for 12–14 h at 4°C. Complete cleavage was verified by SDS-PAGE. A construct of BakΔTM with an N-terminally fused Bad-BH3 domain (BakΔTM-Bad-BH3) was cloned by introducing Bad-BH3 residues 103 to 126 (amino acid sequence: N_{103}LWAAQRYGRELRRMSDEFVDSFK$_{126}$) into BakΔTM by replacing BakΔTM

residues Gly4 to Cys14 that are part of the unfolded N-terminal tail of Bak. Purification of BakΔTM-Bad-BH3 was identical to the procedure for BakΔTM.

Constructs encoding Bak peptides were cloned into an in-house modified pET vector encoding GB1 with N-terminal His_6 tag followed by a thrombin site (His_6-GB1-thrombin-peptide). We produced the following constructs: Bakα1 (residues 24–48), Bak-BH3 (residues 68–88) or Bakα1-BH3 (residues 24–90). For the Bakα1 construct (residues 24–48) that is also used for the pore forming assay (see below), we included an additional TEV site in between the His_6-tag and GB1 to be able to selectively remove the His_6 tag. *E. coli* BL21(DE3) cells harboring the GB1-Bak peptide constructs were grown at 37°C. Protein expression was induced with 1 mM IPTG at OD_{600} 0.7–0.9 and cells were shaken for a further 4 h at 37°C. Cell pellets were resuspended in lysis buffer (50 mM Tris pH 8, 200 mM NaCl, 1 mM ethylenediaminetetraacetic acid (EDTA)) supplemented with lysozyme, a tablet of cOmplete EDTA-free protease inhibitor cocktail and 1 mM phenylmethylsulfonyl fluoride (PMSF). The cell suspension was sonicated for 30 min (1-s pulse, 3-s pause, 30% amplitude) on ice. Following incubation with DN*ase* I and 5 mM $MgCl_2$, cell debris was removed via centrifugation (18 000 g, 30 min, 4°C) and the supernatant was applied to a 1 mL Ni-NTA gravity flow column equilibrated with buffer A (20 mM Tris pH 8, 100 mM NaCl, 5 mM β-mercaptoethanol (BME)). The column was washed with 20 CV buffer A and 20 CV of buffer A + 10 mM imidazole followed by elution with 10 CV of buffer A + 400 mM imidazole. 5% glycerol was added to the elute before concentration for SEC on an ÄKTA Pure system equipped with a HiLoad 16/600 Superdex 75 pg (S75) column equilibrated with 20 mM NaPi pH 7, 50 mM NaCl, 0.1 mM EDTA and 5 mM BME. EDTA was omitted from the SEC buffer with Bakα1 to be used in the liposome permeabilization assay. Here, following SEC, TEV protease was added (1:40 M ratio) for removal of the His_6 tag, followed by reverse Ni-NTA gravity flow affinity chromatography to separate the His_6 tag from the GB1-Bak construct. Successful cleavage was verified by SDS-PAGE. To produce *U*-[^{2}H,^{15}N]-BakΔTM and BclxLΔTM, *E. coli* BL21(DE3) cells were grown in M9 medium supplemented with 1 g/L [98% ^{15}N]-NH_4Cl and 2 g/L ^{1}H,-glucose in >90% D_2O. For the production of *U*-[^{15}N]-Bakα1 and Bakα1-BH3, bacteria were grown in M9 medium supplemented with 1 g/L [98% ^{15}N]-NH_4Cl. For the production of *U*-[^{13}C, ^{15}N]-Bakα1, bacteria were grown in M9 medium supplemented with 1 g/L [98% ^{15}N]-NH_4Cl and 2 g/L [98% ^{13}C]-glucose. Site-directed mutagenesis was performed using the QuikChange lightning kit to introduce the mutations V27C, Q47C or F35A into the Bakα1 fusion-peptide.

Preparation of liposomes

The following lipid composition (mass percentage) was used to mimic the outer mitochondrial membrane (OMM).[46] The OMM-like lipids were prepared by mixing 38% L-α-phosphatidylcholine (PC), 25% L-α-phosphatidylethanolamine (PE), 10% L-α-phosphatidylinositol (PI), 10% 1,2-dioleyl-*sn*-glycero-3-phospho-L-serine (DOPS), 7% 1,1′,2,2′-tetra-(9Z-octadecenoyl)cardiolipin and 10% 18:1 DGS-NTA (Ni^{2+}). For the liposome permeabilization assay at low BakΔTM concentrations (not auto-active), 5% 18:1 DGS-NTA (Ni^{2+}) was used, and the mass of PC was adjusted to compensate. The OMM-like lipids were mixed (1–10 mg) in chloroform and dried under nitrogen gas flow. The lipids were resuspended in 0.25–1 mL of respective buffer, sonicated in a sonication bath until homogeneous then subjected to five freeze and thaw cycles. Finally, the suspension was extruded using a 100 nm polycarbonate membrane. Liposomes containing *E. coli* polar lipids with 5% 18:1 DGS-NTA (Ni^{2+}) used for HDX-MS experiments were prepared identically.

Preparation of phospholipid nanodiscs

Phospholipid nanodiscs were prepared as previously described.[38] Here, we used MSP1D1ΔH5-nanodiscs containing 5% Ni-lipids. The nanodiscs for binding to BakΔTM were prepared with *E. coli* polar lipids and four 18:1 DGS-NTA (Ni^{2+}) lipids per nanodisc, with an MSP:lipid ratio of 1:25. Briefly, a 500 μM stock of MSP1D1ΔH5-nanodiscs were prepared in MSP buffer (20 mM Tris pH 7.5 and 100 mM NaCl), a 50 mM stock of *E. coli* polar lipids containing 5% Ni-lipids was prepared in MSP buffer supplemented with 100 mM sodium cholate. The reaction was assembled in the following order with final concentrations noted in parentheses: MSP buffer, MSP buffer supplemented with 100 mM sodium cholate (sodium cholate up to 20 mM), *E. coli* polar lipids (8 mM) and MSP1D1ΔH5 (0.15 mM). The reaction was incubated at room temperature for 1 h. Subsequently, sodium cholate was removed by adding 0.6 g/mL of Bio-Beads-SM2 to the reaction mixture and incubating at 4°C on a rotary shaker for 2 h. Nanodiscs were purified by SEC on a HiLoad 16/600 Superdex 200 pg (S200) column equilibrated with 20 mM Tris pH 7.5, 100 mM NaCl, and 5 mM BME. A 100 μM stock solution of BakΔTM (0.05 mM final concentration) was added to empty Ni-NTA-nanodiscs to a 1:1 M ratio (0.05 mM nanodiscs) to produce membrane attached Bak. This complex was concentrated to ∼100μM and used for further experiments.

Liposome permeabilization assay

The liposome permeabilization assay was performed at 30°C as previously described.[46,47] 200 nM BakΔTM, 50 nM cBid and 10–200 μM Bakα1 peptide were used for measurements at low BakΔTM concentrations, whereas 1 μM BakΔTM, BakΔTMΔα1, or BakΔTM-Bad-BH3 and 0.125–2 μM BclxLΔTM were used for measurements under auto-active BakΔTM conditions. Bakα1 peptide was titrated into the Bak-BclxL complex from 10 to 100 μM under auto-active conditions. The liposomes were prepared as described above with the addition of the polyanionic dye 8-aminonaphthalene-1,3,6-trisulfonic acid (ANTS) and the cationic quencher *p*-xylene-bis-pyridinium bromide (DPX) as described.[46,47] For experiments at low BakΔTM concentrations, 0.05 mg/mL OMM-like lipids doped with 5% (w/w) 18:1 DGS-NTA (Ni^{2+}) were used. For measurements under auto-active BakΔTM conditions, 0.3 mg/mL OMM-like lipids doped with 10% (w/w) 18:1 DGS-NTA (Ni^{2+}) were used.

Hydrogen deuterium exchange mass spectrometry (HDX-MS)

An ACQUITY UPLC M-class system with automated HDX technology was used and HDX kinetics were measured at 20°C with data points from 0 to 7200 s in technical triplicates. Typically, 4 mg of *E. coli* polar lipids supplemented with 0.5 mg 18:1 DGS-NTA (Ni^{2+}) lipid were used. All samples (30 μM BakΔTM with or without 30 μM BclxLΔTMΔHis_6) were diluted 1:20 in 99.9% D_2O-containing 20 mM NaPi pH 6.8 (or H_2O-containing reference buffer) at the respective HDX kinetic data points. The reaction was quenched by the 1:1 addition of 200 mM KH_2PO_4, 200 mM Na_2HPO_4 pH 2.3, 4 M guanidine hydrochloride, and 200 mM tris(2-carboxyethyl) phosphine (TCEP) at 1°C. 50 μL of sample was applied to an Enzymate BEH pepsin column for on-column peptic digestion at 20°C. The resulting peptides were separated by reversed-phase chromatography using a stepwise gradient of acetonitrile: 5 to 35% in 6 min, 35 to 45% in 1 min, and 40 to 95% in 1 min. A UPLC C18 1.7 μm VanGuard trapping column and a UPLC BEH C18 1.7 μm separation column were used for peptide separation and the elutes were analyzed using an in-line Synapt G2-S QTOF HDMS mass spectrometer. Mass spectroscopy data was collected over an m/z range of 100–2000 and peptides were identified by MSE ramping the collision energy automatically from 20 to 50 V. Data were analyzed using the PLGS 3.0.3 and DynamX 3.0 software packages.

Isothermal titration calorimetry (ITC)

For ITC measurements, BclxLΔTM, GB1- Bakα1-BH3 and GB1-BH3 were dialyzed (MWCO 3 kDa) against 1 L ITC buffer (20 mM NaPi pH 7, 50 mM NaCl, 0.5 mM EDTA, 1 mM DTT) for 12–14 h at 4°C. Dialyzed samples were diluted with ITC buffer to final concentrations of 6–7 μM BclxLΔTM, 139 μM GB1- Bakα1-BH3 and 131 μM GB1-BH3. All ITC measurements were performed on a MicroCal PEAQ-ITC instrument at 25°C. The experimental settings include one 0.4 μL injection followed by 19 2 μL injections with 120 s spacing for equilibration. Data was analyzed with MicroCal PEAQ-ITC analysis software using the one-set-of-sites binding model. Three technical replicates were performed for an error estimation.

Circular dichroism (CD) spectroscopy

Measurements were conducted on a Jasco J-715 spectropolarimeter with a 1 mm path-length quartz cuvette. Spectra were measured at 20°C with concentrations ranging from 10 to 12 μM in SEC buffer (see above, protein expression and purification) and converted to mean residue (MRW) ellipticity units. Thermal unfolding traces were measured by monitoring the ellipticity at 207 nm with a heating rate of 1 °C/min. The thermal melting curves were presented as normalized ellipticity values at 207 nm [0; 1].

NMR spectroscopy

All NMR experiments were measured in 20 mM NaPi pH 6.5, 50 mM NaCl, 0.1 mM EDTA and 5 mM DTT on Bruker Avance III instruments operating at 600, 800, 900 and 950 MHz proton frequency equipped with cryogenic probes. For experiments involving 18:1 DGS-NTA (Ni^{2+}) lipids, EDTA and DTT were omitted from the buffer.

Nanodisc-attached proteins samples were measured with 2D-[^{15}N, ^{1}H]-TROSY experiments, soluble protein samples were measured with 2D-[^{15}N, ^{1}H]-HSQC experiments, and titrations were monitored with a series of 2D-[^{15}N, ^{1}H]-HSQC experiments at 303 K in the respective buffers. Typically, we recorded 48 transients per increment with 128 complex points in the indirect ^{15}N dimension. NMR paramagnetic relaxation enhancement (PRE) experiments[55] were conducted with PROXYL-labeled GB1-Bakα1 single-cysteine peptides (V27C or Q47C), where the spin label was located either at the N- or C-terminal end of the peptide. The spin labeling reaction was done in 20 mM Tris pH 8, 100 mM NaCl, 1 mM EDTA with a 12 mM PROXYL (3-(2-Iodoacetamido)-PROXYL, Merck) stock solution in acetonitrile added to 100 μM of each protein construct in a 10-fold molar excess and incubated 2 h at room temperature. Excess spin label was removed by dialysis against 20 mM Tris pH 8, 100 mM NaCl, 1 mM EDTA with 3.5 MWCO, followed by S75 SEC purification into NMR buffer. A complex of 150–200 μM *U*-[^{2}H,^{15}N]-labeled BclxLΔTM and a 10-fold molar excess of each of the PROXYL-labeled Bakα1 peptides (oxidized sample) was used for the acquisition of 2D-[^{15}N,^{1}H]-HSQC experiments at 303K and 950 MHz proton frequency, using 32 transients and 128 complex points in the ^{15}N dimension, and a recycle delay of 2 s. As a reference, the same experiment was recorded after the addition of 10 mM ascorbic acid to reduce the free radical in the spin label (reduced sample). The PRE effect was depicted with the intensity ratio of the NMR signals between the oxidized and the reduced sample. For backbone assignment, we used a 280 μM ^{13}C, ^{15}N-labeled GB1-Bakα1 peptide sample in 20 mM NaPi pH 6.0, 50 mM NaCl, 0.1 mM EDTA and 5 mM DTT, 0.02% NaN_3, 2 mM PMSF, and recorded a standard set of triple resonance experiments (HNCO, HNCA, HNCOCA, HNCACB)[56] at 303 K and 600 MHz proton frequency. The obtained ^{13}C-chemical shift information was utilized to obtain sequence specific backbone resonance assignments of Bakα1, using the previously published backbone assignments of activated BakΔTM in lipid nanodiscs[17] as a starting point.

Molecular docking

A structural model of the BclxL-Bakα1 complex was constructed by first extracting Bakα1 from the crystal structure of the soluble domain of Bak (residues 24–48 taken from PDB: 2IMS[44]). Bakα1 was then structurally aligned with the structure of BclxL bound to the Bak-BH3 helix (PDB: 1BXL[34]) using Chimera.[57] For this, the NMR chemical shift perturbation data with ^{15}N-labeled Bakα1 after the addition of unlabeled BclxL was used to identify the binding site of BclxL in Bakα1, which was used for the structural alignment with Bak-BH3. This structural alignment procedure resulted in a complex structural model that is consistent with the NMR data. To equilibrate the structural model, we subsequently performed an extended (3 μs duration) molecular dynamics simulation at 303K using

GROMACS Version 2023.3[58]. Input files were generated by the CHARMM-GUI server.[58,59] Analysis of the trajectory to extract the root-mean-square devation (RMSD) of the complex and backbone root-mean-square fluctuation (RMSF) values of Bakα1 in the complex was performed with VMD[60] and GROMACS.[61]

QUANTIFICATION AND STATISTICAL ANALYSIS

Liposome permeabilization assay data analysis

The data were averaged from three technical replicates (N = 3), unless there was a clear outlier due to experimental artifacts. Data analysis was performed by first normalizing to the minimum value for each assay condition. The difference in fluorescence at time point 5,500 s and 0 s was then calculated and averaged for each technical replicate. The data are represented as relative fluorescence with 100% representing the maximum liposome permeabilization observed for the respective conditions compared in each figure.

ITC data analysis

Data was analyzed with MicroCal PEAQ-ITC analysis software using the one-set-of-sites binding model. Three technical replicates (N = 3) were performed for an error estimation and the standard deviation (SD) is indicated in the respective figure.

NMR spectroscopy data analysis

Chemical shift perturbations in the direct ^{1}H and indirect ^{15}N dimensions were scaled using the distribution of nucleus-specific chemical shift changes in proteins.[54,62] Binding isotherms were fitted using a full binding model accounting for the relatively high protein concentrations required for NMR studies.[63] In cases of severe line broadening, binding isotherms were represented as normalized data height. Binding affinities from several residues were calculated for an error estimation and the SD is indicated in the respective figures.